"BABES-BOLYAI" University

Faculty of Physics

Study of some tellurite oxide systems doped with rare earth ions (Eu, Gd) and transition metal ions (Fe, Cu, Mn)

PH.D THESIS

(Summary)

Ph.D

Benta (Dehelean)

Augusta-Adriana

Scientific supervisor

Prof. Univ. Dr. Eugen Culea

Cluj-Napoca

2011

CONTENTS

LIST OF PUBLICATIONS

1. S. Rada, **A. Dehelean**, E. Culea, *Dual role of the six-coordinated lead and copper ions in structure of the copper–lead-tellurate glasses*, Journal of Alloys and Compounds, Volume 509, Issue 2, (2011), 321-325

2. S. Rada, **A. Dehelean**, M. Stan, R. Chelcea, E. Culea, *Structural studies on iron–tellurite glasses prepared by sol–gel method*, Journal of Alloys and Compounds, Volume 509, Issue 1, (2011), 147-151

3. S. Rada, R. Chelcea, M. Culea, **A. Dehelean**, E. Culea, *Experimental and theoretical investigations of the copper–lead–germanate glasses*, Journal of Molecular Structure, Volume 977, Issues 1-3, (2010), 170-174

4. S. Rada, **A. Dehelean**, E. Culea, *FTIR, Raman and UV-VIS spectroscopic and DFT investigation of the structure of iron-lead-tellurate glasses*, Journal of Molecular Modelling, Volume 17, Nr. 8 (2011) 2103-2111

5. S. Rada, **A. Dehelean**, M. Culea, E. Culea, *Dinuclear manganese centers in the manganese-lead-tellurate glasses*, Spectrochimica Acta Part A: Molecular and Biomolecular Spectroscopy, doi:10.1016/j.saa.2011.02.025

6. S. Rada, **A. Dehelean**, E. Culea, *FTIR and UV-VIS spectroscopy investigation on the europium-lead-tellurate glasses*, Journal of Non-Crystalline Solids, Volume 357, Issues 16-17 (2011) 3070-3073

7. **A. Dehelean** and E. Culea, *Magnetic studies of TeO2-Fe2O3 glass systems obtained by the sol-gel method*, Journal of Physics: Conference Series 182 (2009) doi: 10.1088/1742-6596/182/1/012063

8. **A. Dehelean** and E. Culea, *Magnetic behaviour of europium ions in some tellurite glasses obtained by the sol-gel method*, Journal of Physics: Conference Series 182 (2009) doi: 10.1088/1742-6596/182/1/012064

9. **A. Dehelean**, Rada Simona, Popa Adriana, Danciu Virginia, Culea Eugen, *FTIR and EPR spectroscopic characterisation of iron-tellurite glasses obtained by the sol-gel method*, Progress of Cryogenics and Isotopes Separation, vol. 13, Issue 1, (2010), 53-64

10. **A. Dehelean**, C. Voica, E. Culea, *Method validation for determination of metals in oxide materials by ICP-MS*, Analytical and Nanoanalytical Methods for biomedical and Environmental Sciences, Proceedings of IC-ANMBES 2010, Transilvania University Press, 2010, ISBM: 978-973-598-722-0

INTRODUCTION

Tellurite oxide systems attracted attention of researchers, especially for applications such as optical and acoustic materials in photo-chromic glasses or laser technology. Tellurite glasses are very interesting materials due to their broadband transmission in the vicinity of 1.55 μm wavelength and high non-linear third order optical susceptibility (50 times higher than one of SiO2 systems). The tellurite glasses are of technical interest due to high refractive index, high transmittance from ultraviolet to near infrared, low glass transition temperature and electrical semiconductivity and do not have the hygroscopic properties which restrict the applications of phosphate and borate glasses.

Solids doped with rare earth ions are an important class of optical systems which attract more and more attention to the researchers, evidenced by the multitude of studies reported in literature. The successful development of numerous glasses containing rare earth ions resulted in a lot of technological applications in telecommunications (optical communications, lasers, sensors, signal amplifiers, fiber laser emission).

Also, vitreous systems derived from heavy metal oxides have found applicability in many important fields like optoelectronics, especially due to their high refractive index, high density and low phonon energies.

The processing route mainly adopted for producing oxide glasses is a melting and quenching technique. Since the diffusion of reactants in the solid phase is very slow, reaction of this type require high temperatures and long periods of time, conditions that can cause unwanted incorporation of impurities and microstructure in the final product.

In recent years, the sol-gel method is increasingly used to obtain materials with improsed properties. The sol-gel synthesis is a non-traditional method which does not imply the melting of an oxide. It is limited to the heat treatment in the final stage near the glass transition temperature considerably lower than the melting temperature of oxides. The glass synthesis by sol-gel method involves chemical reactions and is based on inorganic polymerization of precursors. This method allows the preparation of higher purity material due to a better homogenization of the initial mixture by mixing at molecular scale.

Doctoral thesis is based on the preparation of tellurite glasses using the melting/quenching and sol-gel methods with structural characterization of the materials by spectroscopic methods.

The thesis is structured in five chapters, conclusions and references. In chapter 1 the general concept regarding vitreous oxide materials and preparation methods are presented.

Chapter 2 presents the theoretical aspects of some experimental methods used in the analyses of vitreous structure, like: X-ray diffraction, IR, Raman, UV-Vis and Electron Paramagnetic Resonance (EPR) spectroscopy.

Chapter 3 describes the sol-gel method used to obtain tellurite materials studied in this work. Chapters 4 and 5 are original results obtained in studies on tellurite oxide systems doped with rare earth ions and transition metals obtained by melting and quenching technique and sol-gel method.

EXPERIMENTAL RESULTS

CHAPTER 4. Characterization of some tellurite glasses obtained by melt/quenching method

4.1. The preparation and processing of the samples

The glass systems: $xEu_2O_3 \cdot (100-x)[4TeO_2 \cdot PbO_2]$ with $0 \leq x \leq 40$ mol %, $xFe_2O_3 \cdot (100-x)[4TeO_2 \cdot PbO_2]$ with $0 \leq x \leq 60$ mol %, $xCuO \cdot (100-x)[4TeO_2 \cdot PbO_2]$ with $0 \leq x \leq 40$ mol %, $xMnO \cdot (100-x)[4TeO_2 \cdot PbO_2]$ with $0 \leq x \leq 40$ mol %, were prepared using reagent grade compounds, i.e. $(NH_4)HPO_4$, TeO_2, PbO_2, Eu_2O_3, Fe_2O_3, CuO, MnO in suitable proportions. The mixtures corresponding to the desired compositions were mechanically homogenized, placed in sintered corundum crucibles and melted in air in an electric furnace at 875 ℃. The molten material was kept at this temperature for 10 minutes and then quenched at room temperature by pouring on the stainless-steel plates.

The structure of the samples were analyzed by X-ray diffraction, using powders, with a D8 Advance Bruker diffractometer.

Density measurements were made using the pycnometer method.

Infrared spectra were obtained in the 400-4000 cm^{-1} spectral range and it was analyzed especially in the 400-1200 cm^{-1} regions with a JASCO 6100 FT-IR spectrometer by using the KBr pellet technique. The spectral resolution used for the recording of the IR spectra was 2 cm^{-1}. In order to obtain good quality spectra, the samples were crushed in an agate mortar to obtain particles of micrometer size. This procedure was applied every time to fragments of bulk glass to avoid structural modifications due to ambient moisture.

UV-Vis absorption spectra of the powdered glass samples were recorded at room temperature in the range 250-1000 nm using Perkin-Elmer Lambda 45 UV/VIS spectrometer. These measurements were made on glass powder dispersed in KBr pellets.

The Raman spectra were collected at room temperature using a JASCO NRS-3300 micro-Raman Spectrometer with an air cooled CCD detector in a backscattering geometry and using a 600/mm grating. The microscope objective used for the studies was 100X. As excitation, it was used a 785 nm laser line with the power at the sample surface of 85 mW.

EPR measurements were carried out at room temperature using a Bruker ELEXSYS E500 spectrometer in X - band (9.4 GHz) and with a field modulation of 100 kHz. To avoid the alteration of

the glass structure due to the ambient conditions, samples of equal quantities were enclosed immediately after preparation in quartz tubes of the same caliber.

4.2. xEu$_2$O$_3$·(100-x)[4TeO$_2$·PbO$_2$] glass systems

4.2.1. Density measurements

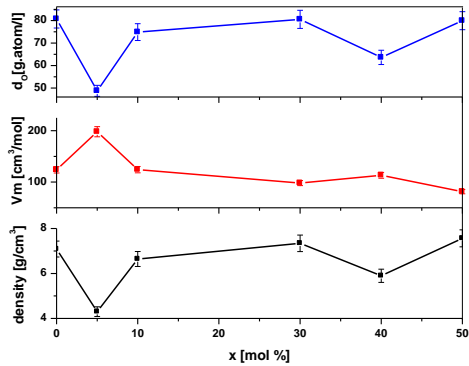**Fig. 4.1.** Europium oxide composition dependence on a) density; b) molar volume, Vm and c) the oxygen packing density, d$_O$, for xEu$_2$O$_3$·(100-x)[4TeO$_2$·PbO$_2$] glasses with 0≤x≤50 mol%.

The compositional variation of the density of glasses is important, especially in the context of the study of structural changes. Thus, the abrupt changes of the density of a glass suggest important structural modifications of the vitreous network.

By adding a low Eu$_2$O$_3$ content (5 mol %) to the host matrix, the formation of non-bridging oxygens is generated. The conversion of some [TeO$_4$] to [TeO$_3$] structural units yields a surplus of non-bridging oxygen atoms, too. Consequently, the density, d, and oxygen parking density, d$_0$, decrease while the molar volume, V$_m$, increases.

Figure 4.1. shows the presence of density maxima at x=30 mol % Eu$_2$O$_3$. For the sample with x = 30 mol % the molar volume decreases and the oxygen packing density increases. This behavior can be explained considering that the addition of modifier europium ions to the lead tellurite glasses introduces an oxygen surplus into the vitreous network. The additional oxygen may be incorporated by the conversion of lead atoms from a lower to a higher coordination.

4.2.2. FTIR spectroscopy

The examination of the FTIR spectra of the xEu$_2$O$_3$·(100-x) [4TeO$_2$·PbO$_2$] glasses up to x=0-50 mol % (Figure 4.2.) shows that the increase of Eu$_2$O$_3$ content strongly modifies the characteristic IR bands. The bands located in the 400-500 cm^{-1} region are attributed to the bending mode of Te-O-Te linkages which may be overlapped with that assigned to the bending mode of the Pb-O-Pb stretch in the [PbO$_4$] structural units [1-7].
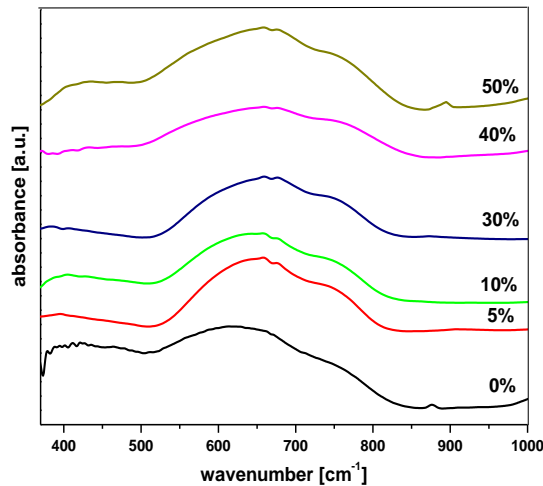
Fig. 4.2. FTIR spectra of $xEu_2O_3 \cdot (100-x)[4TeO_2 \cdot PbO_2]$ glasses with $0 \leq x \leq 50$ mol%.

The band situated in the 720-780 cm^{-1} region indicates the presence of $[TeO_3]$ units [8, 9].

The larger band centered at 620 cm^{-1} is assigned to the stretching mode of $[TeO_4]$ structural units with bridging oxygens [10, 11].

By increasing the Eu_2O_3 content up to 10 mol %, this band shifts to higher wavenumbers, indicating the conversion of some $[TeO_4]$ into $[TeO_3]$ structural units. It seems that the content of $[TeO_4]$ structural units cannot become higher, because the modified $[TeO_3]$ units containing one or more Te-O-Pb bonds are unable to accept a fourth oxygen atom. This compositional evolution of the structure could be explained considering that the excess of oxygen may be accommodated by the formation of $[PbO_3]$ and $[PbO_4]$ structural units.

The broader band centered at 670 cm^{-1} and shoulder located at about 870 cm^{-1} can be attributed to Pb-O bond vibrations from $[PbO_3]$ and $[PbO_4]$ structural units [3, 4].

4.2.3. UV–VIS spectroscopy

Figure 4.3. presents FTIR spectra obtained for $xEu2O3 \cdot (100-x)[4TeO2 \cdot PbO2]$ glasses with $0 \leq x \leq 50$ mol% .

The Pb^{+2} ions with s^2 configuration strongly absorb in the ultraviolet and cause broad emission bands in the ultraviolet and blue spectral area. The intense band obtained at about 310 nm corresponds to the Pb^{+2} ions [12].

The broad UV absorption bands located between 250 and 340 nm are assumed to originate from the host glass matrix. The strong transitions in the UV–VIS spectrum can be due to the presence of the Te-O bonds from $[TeO_3]$ structural units and the Pb-O bonds from $[PbO_3]$ structural units which allow n–π∗ electronic transitions.
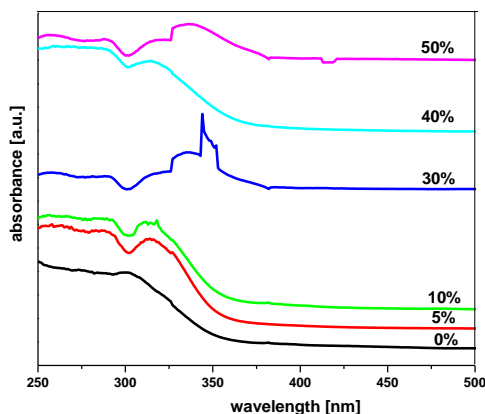
Fig. 4.3. UV–VIS absorption spectra of $xEu_2O_3 \cdot (100-x)[4TeO_2 \cdot PbO_2]$ glasses in function of europium oxide content

For the samples with $x \geq 30$ mol% Eu_2O_3, new bands located in the region between 340 and 400 nm appear in the UV–VIS spectra. These bands can be assigned to the Eu^{+3}–Eu^{+2} conversions. The sharp peak centered at about 390 nm is a band characteristic of Eu^{+3} ($^3F_0 \rightarrow {}^5L_6$) while the shoulder rising into the UV is due to Eu^{+2} ions.

The Eu^{+3}–Eu^{+2} conversion processes attain the maximum value for the samples with x=30 and 50 mol % Eu_2O_3. Based on these experimental results, we propose the following possible redox reactions:

$Pb^{+2} \leftrightarrow Pb^{+4} + 2e^-$

$2Eu^{+3} + 2e^- \leftrightarrow 2Eu^{+2}$
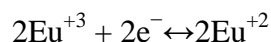
4.3. $xFe_2O_3 \cdot (100-x)[4TeO_2 \cdot PbO_2]$ glass systems

4.3.1. FTIR spectroscopy

Figure 4.4. shows FTIR spectra of Fe_2O_3-doped lead–tellurate glasses.

The larger band centered at ~625 cm^{-1} is assigned to the stretching mode of the trigonal bipyramidal [TeO_4] with bridging oxygens. The shoulder located at about 750 cm^{-1} indicates the presence of [TeO_3] structural units. For all of the glasses, the general trend is a shift towards higher wavenumbers (668 cm^{-1}) with Fe_2O_3 content. This suggests the conversion of some [TeO_4] to [TeO_3] structural units, because the lead ions have a strong affinity towards these groups containing nonbridging oxygens, which are negatively charged.

The broader band centered at about 670 cm^{-1} can be attributed to Pb–O bond vibrations from [PbO_3] and [PbO_4] structural units [1, 4, 5, 22].

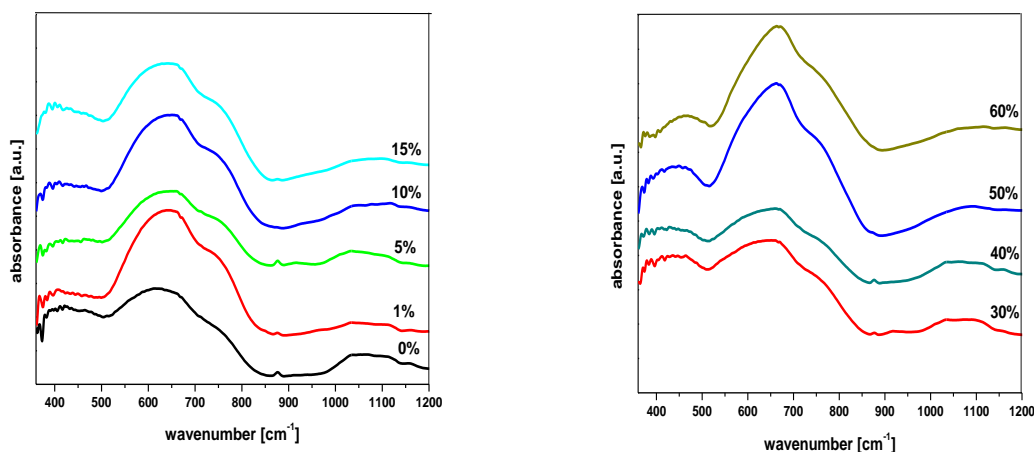Fig. 4.4. FTIR spectra of $xFe_2O_3 \cdot (100-x)[4TeO_2 \cdot PbO_2]$ glasses with $0 \leq x \leq 60$ mol%

With increasing Fe_2O_3 content (up to 15 mol %), the formation of larger numbers of nonbridging oxygens results in the appearance of $[PbO_n]$ structural units (n=3, 4) in the vicinity of the $[TeO_3]$ structural units. The increase in the intensity of the band located at about 600 cm^{-1} corresponding to the Fe-O vibrations from $[FeO_4]$ structural units.

A new band appears at 470 cm^{-1} corresponding to the Fe–O vibrations from the $[FeO_6]$ structural units.

For the sample with $x \geq 30$ mol% Fe_2O_3, the tendency of the bands located in the region between 550 and 850 cm^{-1} to move towards higher wavenumbers can be explained by the conversion of $[TeO_4]$ into $[TeO_3]$ structural units.

4.3.2. Raman spectroscopy

Figure 4.5. shows the Raman spectra of the $xFe_2O_3 \cdot (100-x) [4TeO_2 \cdot PbO_2]$ glasses with x=0–60 mol %.

The bands centered at around 652 cm^{-1} originate from vibrations of the continuous tetragonal bipyramidal $[TeO_4]$ network, and the bands centered at around 710 cm^{-1} are from the $[TeO_{3+1}]$ and $[TeO_3]$ structural units [24]. It was found that the maximum phonon energy of the doped glasses gradually increased from 710 to 745 cm^{-1}.

As the Fe_2O_3 content increases up to 60 mol%, the numbers of polyhedral $[TeO_{3+1}]$ and trigonal pyramidal $[TeO_3]$ structural units increase in the network structure.
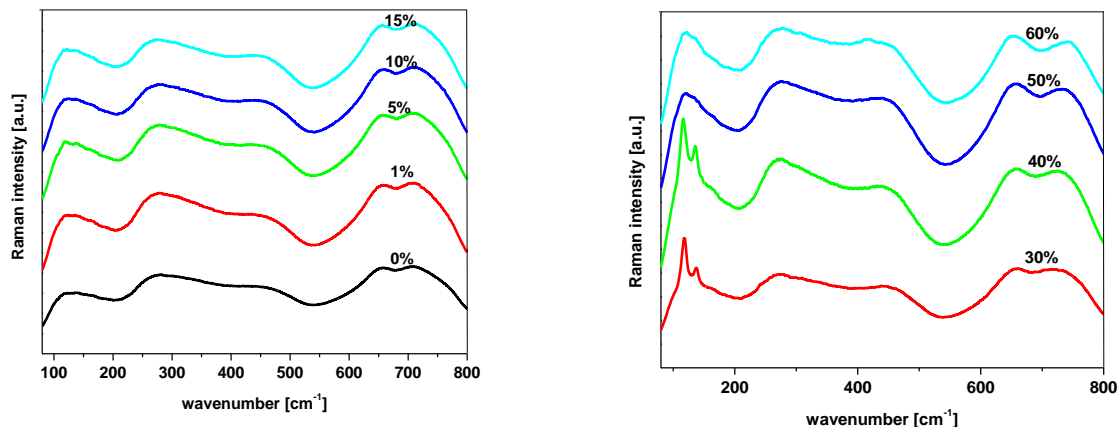
Fig. 4.5. Raman spectra of xFe2O3·(100−x)[4TeO2·PbO] glasses with 0≤x≤60 mol%

The Raman band centered at about 270 cm^{-1} may be associated with Pb–O stretching and O–Pb–O bending vibrations. The strong bands situated near 120 and 135 cm^{-1} in the Raman spectra of iron–lead–tellurate glasses are almost certainly due to Pb–O symmetric stretching vibrations [25, 26]. Support for this comes from the fact that the relative intensity of this band increases with increasing Fe_2O_3 content of the glass from x=1 to 40 mol % Fe_2O_3, but the intensity decreases markedly for higher Fe_2O_3 contents than this. This shows that a high Fe_2O_3 content can lead to broken Pb–O bonds in iron–lead–tellurate glasses. On the other hand, this is necessary because the content of [TeO$_3$] structural units increases.

Table 4.2. Assignment of the Raman and IR bands for xFe_2O_3·$(100-x)[4TeO_2·PbO]$ glasses

Raman band (cm^{-1})	FTIR band (cm^{-1})	Assignment
120, 135	-	vibratii simetrice de stretching in legaturi Pb–O [25, 26]
270	-	vibratii de stretching in legaturi Pb–O si vibratii de bending in legaturi O–Pb–O [25]
-	400–500	vibratii ale legaturii Fe–O in [FeO$_6$] [22]
405	470	vibratii ale legaturii Pb–O in [PbO$_4$] [22]
465	475	vibratii de stretching in legaturi Te–O–Te [23]
-	570–600	vibratii ale legaturii Fe–O in [FeO$_4$] [4]
650–670	620–680	vibratii de stretching in [TeO$_4$] [24]
-	670, 850, 1050	vibratii ale legaturii Pb–O in [PbO$_3$] si [PbO$_4$] [1, 5]
720–735	720–780	vibratii de stretching in [TeO$_3$]/[TeO$_{3+1}$] [24]

By increasing of Fe_2O_3 content up to 40 mol %, the intensity of the band situated at 135 cm^{-1} attains its maximum value. We think that a higher doping level can result in broken Pb–O bonds and cause the [PbO$_4$] structural units to change to [PbO$_3$] chains [27]. For the sample with x=60 mol%, a supplementary, well-defined Raman band appears at around 415 cm^{-1}. This band is due to covalent Pb–O bond vibrations [28, 29].

For higher Fe_2O_3 contents, the Raman spectra indicate a greater degree of depolymerization of the vitreous network than the FTIR spectra do.

4.3.3. UV-Vis spectroscopy

The UV-Vis absorption spectra of $xFe_2O_3 \cdot (100-x)$ [4TeO$_2$·PbO$_2$] glasses with x=0–60 mol% are shown in Figure 4.6.
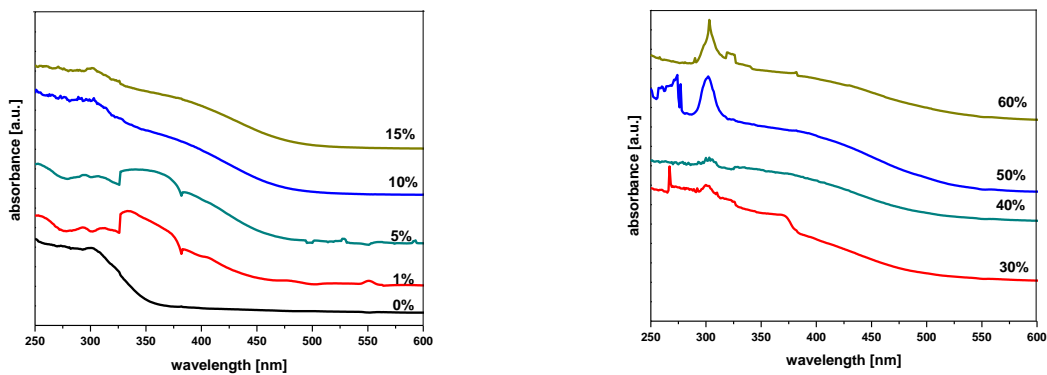
Fig. 4.6. UV-Vis absorption spectra of $xFe_2O_3 \cdot (100-x)$[4TeO$_2$·PbO$_2$] glasses as a function of iron oxide content

The stronger transitions in the UV-Vis spectrum may be due to the presence of Te=O bonds from [TeO$_3$] structural units and Pb=O bonds from [PbO$_3$] structural units, which allow n–π* transitions. Pb^{2+} ions with the s^2 configuration absorb strongly in the ultraviolet and yield broad emission bands in the ultraviolet and blue spectral regions. The intense band centered at about 310 nm corresponds to these Pb^{2+} ions [38].

Upon introducing a low content of Fe_2O_3 (x≤5 mol%) into the host matrix, new UV absorption bands appear. These bands, located in the 320–450 nm region, are due to the presence of the Fe^{3+} ions. The intensity of the absorption band located at about 250 nm increases, and the iron in some cases is reduced to Fe^{2+} through electron trapping [39]. Some weak bands appear in the 450–550 nm region. These bands show that some Fe^{3+} ions were converted to Fe^{2+} ions. Based on these experimental results, we propose the following possible redox reactions:

$2Fe^{3+} + 2e^- \leftrightarrow 2Fe^{2+}$

$Pb^{2+} \leftrightarrow Pb^{4+} + 2e^-$
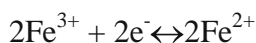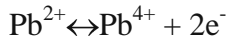
  The increased intensity of the band situated near 300 nm can be attributed to the formation of new Pb=O bonds from [PbO_3] structural units.

  For the sample with x=30 mol% Fe_2O_3, a new band appears at about 267 nm. This can again be explained by distortions of the iron species. It is possible that [FeO_6] is converted to [FeO_4] structural units.

  For the sample with x=60 mol% Fe_2O_3, the UV absorption bands situated in the 250–290 nm region disappear and new bands appear at 320 nm. These bands show the presence of new Fe^{3+} ions. The kink located at about 430 nm is characteristic of Fe^{3+} ions with octahedral symmetry. Also, it is proposed that some of the Fe^{2+} ions capture positive holes and are converted to Fe^{3+} according to the following photo-chemical reactions:

$Fe^{2+} + \text{positive holes} \rightarrow Fe^{3+}$

$Pb^{4+} + 2e^- \rightarrow Pb^{2+}$
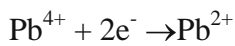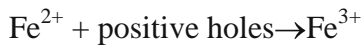
4.3.4. EPR spectroscopy
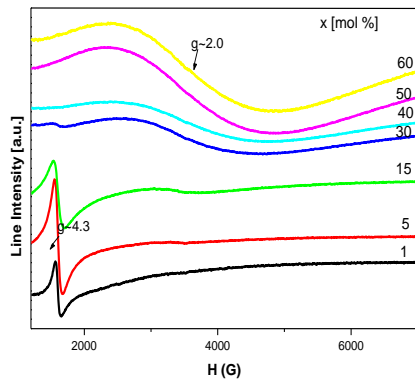
Fig. 4.7. EPR spectra of $xFe_2O_3 \cdot [4TeO_2 \cdot PbO_2]$ glasses with $1 \leq x \leq 60$ % mol

  The Fe^{3+} EPR spectra are characterized by resonance absorptions at g ≈ 4,3 and g ≈ 2,0, their relative intensity depending on the iron content of the samples.

  The resonance line at g ≈ 4,3 is corresponding to the isolated Fe^{3+} ions situated in octahedral, rhombic or tetragonal symmetric distorted neighborhoods. The line from gef ≈ 2,0 is attributed to Fe^{3+} ions involved in magnetic interactions or clusters.
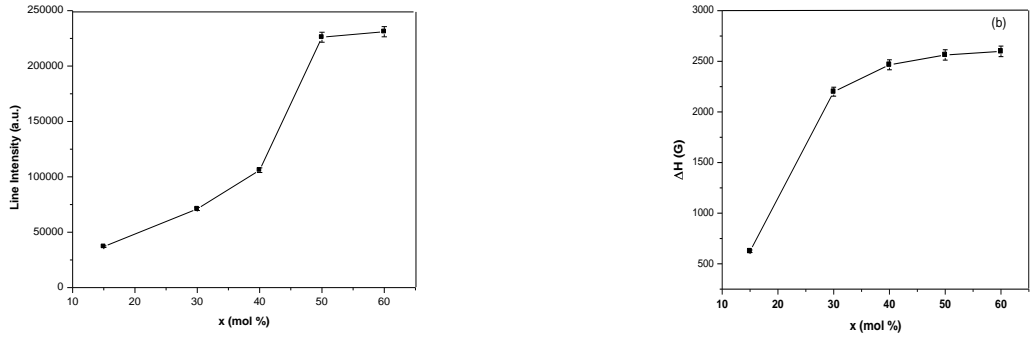
Fig. 4.8. The dependence on Fe_2O_3 content of the intensity (a) and width (b) of resonance line at gef ≈ 2.0 for $xFe_2O_3 \cdot [4TeO_2 \cdot PbO_2]$ glasses with $1 \leq x \leq 60$ % mol

For all investigated sample, the intensity of the resonance line at geff $\approx$ 2.0 (Figure 4.8.a) increases with the increase of x in the whole concentration range. Above 50 mol %, the corresponding increase is very slowly. The non-linear increase of intensity with iron concentration shows that iron ions are present as Fe^{2+} as well as Fe^{3+}. For $15 \leq x \leq 30$ mol %, the linewidth increases (Figure 4.8.b), in this range could appear dipolar interactions. Above 30 mol % the linewidth continue to increase but very slowly and in this range coexist the dipol-dipol and superexchange magnetic interaction and their intensity are ~ equal.
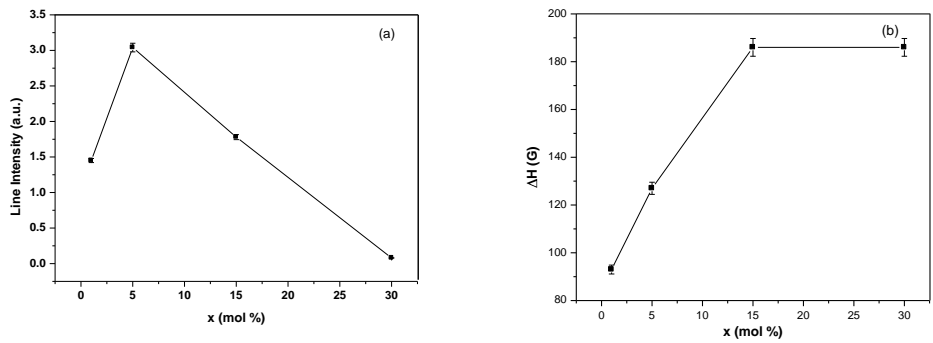
Fig. 4.9. The dependence on Fe_2O_3 content of the intensity (a) and width (b) of resonance line at gef $\approx 4,3$ for $xFe_2O_3 \cdot [4TeO_2 \cdot PbO_2]$ glasses with $1 \leq x \leq 60$ % mol

The intensity of the resonance line at geff $\approx$ 4.3 can be observed as increasing up to 5 mol % (Figure 4.9.a). Over this concentration, the intensity decreases due to decrease in the number of Fe^{3+} ions. The line - width of the resonance line from gef $\approx$ 4.3 (Figure 4.9.b).) increases up to 15 % mol due to Fe^{3+} species interacting by magnetic coupling dipole- dipole as the main broadening mechanism.

Over this concentration line - the width of the resonance line from gef ≈ 4.3 for $xFe_2O_3 \cdot [4TeO_2 \cdot PbO_2]$ glasses decreases due to decrease of Fe^{3+} number and to the structural disorder in glasses with the increase of Fe_2O_3 content.

4.4. xCuO·(100-x)[4TeO₂·PbO₂] glass systems

4.4.1. FTIR spectroscopy
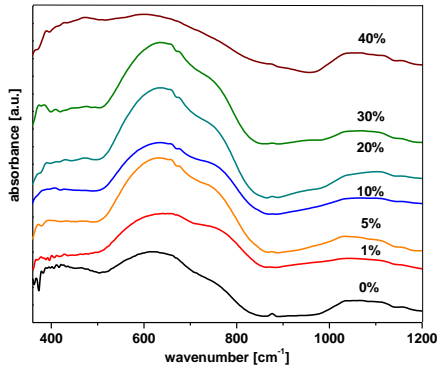
Fig. 4.10. Spectrele FTIR al sistemului vitros xCuO·(100-x)[4TeO₂·PbO₂] pentru $0 \leq x \leq 40$ % mol

Prominent absorption bands located in the 500–800 cm^{-1} region have maxima at 620 cm^{-1} and a shoulder at 760 cm^{-1} in the host matrix. The broad bands situated between 620 and 680 cm^{-1} are assigned to the stretching vibration of equatorial and axial Te–O bonds in the $[TeO_4]$ trigonal bipyramidal units, while the absorption of the $[TeO_3]$ units corresponds to the wavenumber of 720–780 cm^{-1}.

In the host matrix, the absorption band situated at 620 cm^{-1} shifts to higher wavenumbers (630 cm^{-1}) by increasing of CuO content up to 30 mol%. A shift of absorption bands to higher wavenumber indicates the conversion of some $[TeO_4]$ into $[TeO_3]$ structural units, because the lead ions have a strong affinity towards these groups containing non-bridging oxygens, with negative charge.

The broad band centered at about 670 cm^{-1} and shoulder located at about 850 cm^{-1} can be attributed to Pb–O bonds vibrations from $[PbO_4]$ structural units [3, 5, 7, 10, 63-65]. Band centered at about 470cm^{-1} maybe correlated withPb–Ostretching vibration in $[PbO_4]$ structural units [66, 67]. A small peak located at about 875cm^{-1} corresponding to the [PbO6] structural units was observed in the host matrix.

By increasing of CuO content up to 5 mol%, the formation of the larger numbers of non-bridging oxygen's produces the apparition of $[PbO_3]$ and $[PbO_4]$ structural units in the vicinity of the $[TeO_3]$ structural units. Absorption bands located at about 1000 and 1100 cm^{-1} are attributed to Pb–O asymmetric stretching vibrations in $[PbO_n]$ structural units.

The increase of CuO content up to 30 mol% implies the modifications in the intensity of the bands situated in the 500–825 cm^{-1} region. The excess of oxygen may be accommodated by the formation of some [CuO6] structural units, in agreement with UV–Vis data. (v) For sample with x = 40 mol %, the decreasing trend of the bands located in the region between 400 and 800 cm^{-1} can be due to the formation of bridging bonds of Pb–O–Cu and Cu–O–Te.
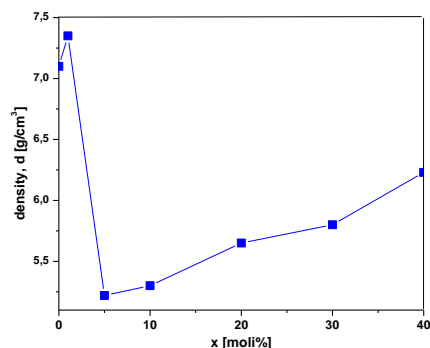
4.4.2. Density measurements

Fig. 4.11. Copper oxide composition dependence on density for xCuO·(100−x)[4TeO$_2$·PbO$_2$] glasses with 0≤x≤40 mol%.

The density increases from 5.22 to 6.23 g/cm^3 when the copper oxide contents of the samples modify from 5 to 40 mol%. The relation between the density and the copper ions content is not linear for the whole field of concentration. Fig.4.11 shows the presence of density maxima at x = 1 and 40 mol % CuO. The addition of the modifier copper (II) oxide to the lead-tellurate glass network introduces surplus oxygen into the vitreous network. The additional oxygen may be incorporated by the conversion of lead atoms from a lower to a higher coordination.

The density decreases abruptly when up to 5 mol% copper oxide was added, showing the formation of Cu–O–Te or Cu–O–Pb linkages.

By increasing the CuO amount up to 40 mol%, the density increases showing the substitution of the [PbO$_6$] structural units by [CuO$_6$] entities. These small [CuO$_6$] entities will create smaller network cavities and subsequent local densification. Consequently the density increases.

4.4.3. UV-Vis spectroscopy

Fig. 4.12. reveals the UV–vis absorption spectra of xCuO·(100−x)[4TeO$_2$·PbO$_2$] glasses.
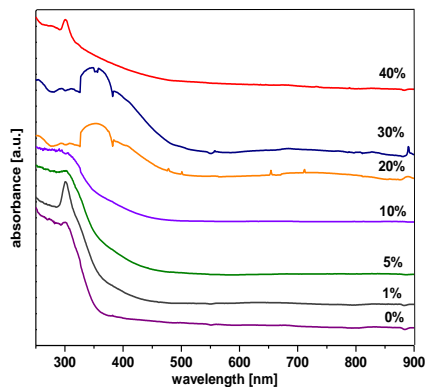
Fig. 4.12. UV–vis absorption spectra of CuO·(100−x)[4TeO₂·PbO₂] glasses in function of copper oxide content.

In the host matrix, the stronger transitions in UV region can be due to the presence of the Te-O bonds from [TeO$_3$] structural units and Pb-O bonds from [PbO$_3$] structural units which allow n–π* transitions. Ions Pb^{+2} absorb strongly in the ultraviolet (310 nm) and yield broad emission bands in the ultraviolet and blue spectral area [12]. The intensity of the UV–vis band located at about 310nm attains maximum value for sample with x = 1 mol % CuO. This shows that the lead ions participate as network former.

For sample with x≥20 mol% CuO, UV spectra exhibit a charge transfer bands due to dπ–pπ–dπ transitions from the tricentric metal–oxygen–metal bonds which is reduced to a shoulder recorded at 255 nm.

By increasing the CuO content up to 30 mol%, new bands appear in the 320–400nm region. The intensity of absorption increases with the concentration of copper ions up to 30 mol%. These broad visible bands indicate that the copper ions in the lead-tellurate glasses are present mostly as Cu^{+2} ions in octahedral symmetry with tetragonal elongation sites. These bands were assigned to the $^2B_{1g}{\to}^2B_{2g}$ transitions of the Cu^{+2} ions present in the axially elongated octahedral sites [76, 77].

For sample with x = 40 mol% CuO, the strong intensity of the bands situated in the 320–900nm domain disappears indicating the reduction of some Cu^{+2} to Cu$^+$ ions.

4.4.4. EPR spectroscopy

The EPR spectra for CuO·(100−x)[4TeO₂·PbO₂] glasses are presented in figure 4.13.

For x≤10 mol % CuO the EPR spectra are asymmetric, characteristic for isolated of Cu^{2+} ions in an axially distorted octahedral environment.

The spectra show the parallel partially resolved hfs due to the interaction of the unpaired electron with the nuclear spin I=3/2 of the Cu^{2+} ion. The perpendicular hfs is not resolved indicating a width of

the individual components exceeding the $|A_\perp|$ separation. For higher concentrations ($x \geq 20$ mol% CuO), EPR spectra show a single absorption line due to clustered ions Cu^{2+}, located at $g \approx 2.1$.
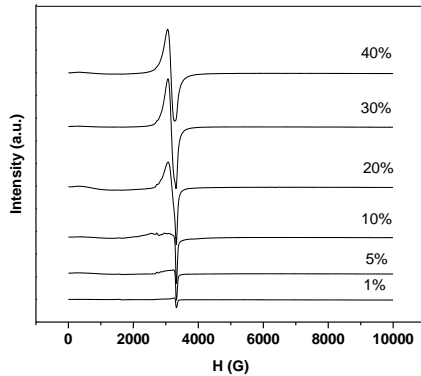

Fig. 4.13. EPR spectra due to Cu^{2+} ions in $xCuO\cdot(100\text{-}x)[4TeO_2\cdot PbO_2]$ glasses for $1 \leq x \leq 40$ % mol
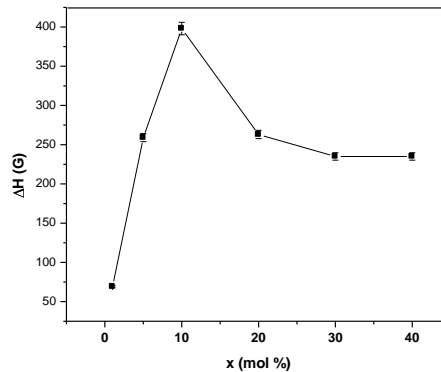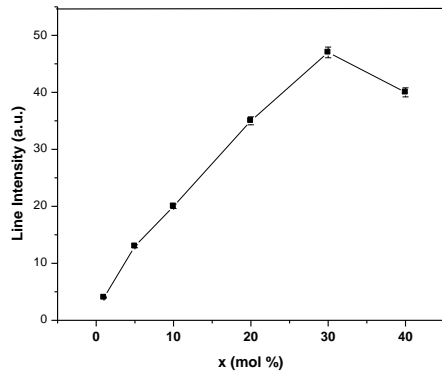
Fig. 4.17. The dependence on CuO content of the intensity (a) and width (b) of resonance line at gef ≈ 2.1 for $xCuO\cdot(100\text{-}x)[4TeO_2\cdot PbO_2]$ glasses for $1 \leq x \leq 40$ % mol

The intensity of the resonance line at geff ≈ 2.1 can be observed as increasing up to 30 mol % (Figure 4.17.a). Over this concentration, the intensity decreases due to decrease in the number of Cu^{2+} ions.

The line width increases with the CuO content up to x= 10 mol % due to the increase of the dipolar interaction between the Cu^{2+} ions. For higher concentrations, x$\geq$10 mol % it could be observed a strong decrease of the linewidth which could be attributed to a superexchange – type interaction between the copper ions. The progressive appearance of Cu^{+} ions in the glass composition is supported by reducing the absorption signal (Fig. 4.17. a))

4.5. xMnO·(100-x)[4TeO₂·PbO₂] glass systems

4.5.1. Density measurements

Fig. 4.18. Manganese oxide composition dependence on a) density; b) molar volume, Vm for xMnO·(100-x)[4TeO$_2$·PbO$_2$] glasses with 0≤x≤40 mol%.

Fig. 4.18. shows the compositional evolution of the density of the manganese-leadtellurate glasses. The relation between the density and 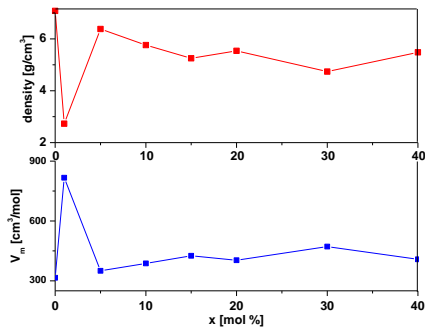the manganese ions content is not linear for the whole field of concentration. The density increases from 2.73 to 6.38 g/cm^3 when the MnO content of the samples modifies from 1 to 5 mol%.

By introduction of low MnO content (1 mol%) in the host matrix, the density decreases abruptly because some [TeO$_4$] structural units were converted to the [TeO$_3$] structural units, in agreement with the IR data (Fig.4.19). For the sample with x=5 mol% the density attains a maximum value. The additional oxygen may be incorporated by the conversion of lead atoms from a lower to a higher coordination. Further the addition of the MnO content up to 20 mol% needs the commodated of the glasses network with the excess of oxygen atoms by the formation of the Te-O-Mn and Pb-O-Mn linkages

4.5.2. FTIR spectroscopy

The experimental FTIR spectra of xMnO·(100-x)[4TeO$_2$·PbO$_2$] glass system with various content of manganese oxide (0 ≤ x ≤ 40 mol%) were presented in Fig. 4.19. The broader bands situated between 620-680cm^{-1} are assigned to the stretching vibration of equatorial and axial Te-O bonds in the [TeO$_4$] trigonal bipyramidal units, while the absorption band of the [TeO$_3$] units corresponds to the wavenumber of 780 cm^{-1}.

The absorption band situated at 620cm^{-1} in the host matrix is shifting to higher wavenumbers (640 cm^{-1}) by increasing of MnO content up to 15 mol %. A shift of absorption band to higher wavenumber indicates the conversion of some [TeO$_4$] to [TeO$_3$] structural units. This can be explained considering that the lead ions have a strong affinity towards these structural units containing non-bridging oxygens with negative electrical charges.

Up to 20 mol% MnO it can be observed that the addition of manganese ions is leading to a broadening of the bands located in the 400-800cm^{-1} region and to a structure more and more disordered.
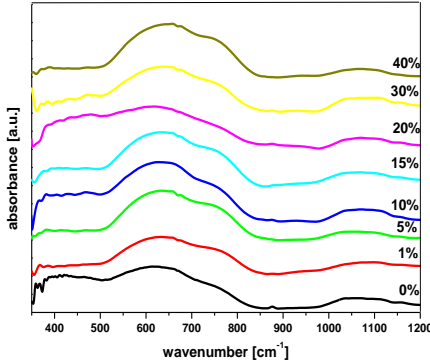

Fig. 4.19. FTIR spectra of xMnO·(100-x)[4TeO$_2$·PbO$_2$] glasses with 0≤x≤40mol%

A sharp of decreasing trend was observed both in frequency and strength of the band from 400-800 cm^{-1}. This might be due to the formation of the Mn-O-Pb and Mn-O-Te bridging bonds. Since the stretching force constant of Mn-O bonding is substantially lower than that of the Te-O and Pb-O, the stretching frequency of Mn-O-Pb and Mn-O-Te might trend to be lower.

By increasing of MnO content up to 30 mol%, the formation of the larger numbers of non-bridging oxygen's yields the apparition of [PbO$_3$] and [PbO$_4$] structural units in the vicinity of the [TeO$_3$] structural units. This band assigned to stretching vibrational mode of [TeO$_3$] structural units increase in intensity by the increasing of MnO content.

4.5.3. UV-Vis spectroscopy

The UV-VIS absorption spectra of xMnO·(100-x)[4TeO$_2$·PbO$_2$] glasses with x=0-40 mol % are shown in Fig. 4.20.

The stronger transitions in the UV-VIS spectrum can be due to the presence of the Te=O bonds from [TeO$_3$] structural units and Pb=O bonds from [PbO$_3$] structural units which allow n-π* transitions. Ions Pb^{+2} with s^2 configuration absorb strongly in the ultraviolet and yield broad emission bands in the ultraviolet and blue spectral area. The intense band centered at about ~300 nm corresponds to the Pb^{+2} ions [12]. The Mn-doped glasses show no characteristic visible bands, but only a small kink at 385nm due to Mn^{+2} ions, which are known to have very low extinction coefficients [38].
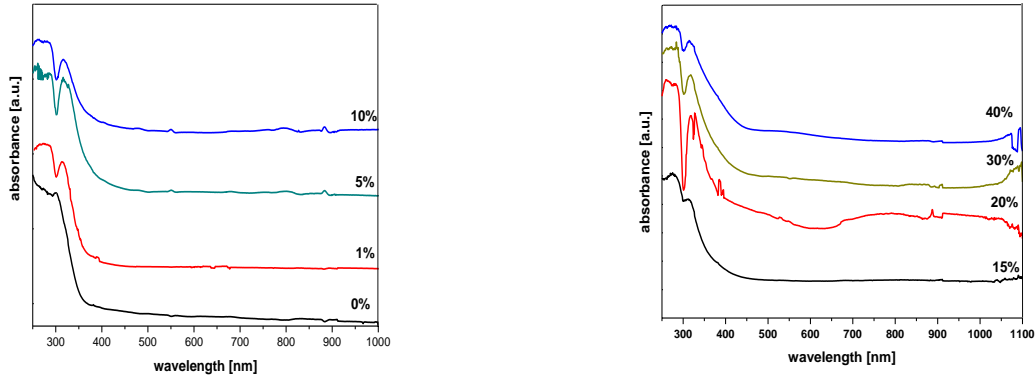
Fig. 4.20. UV-VIS absorption spectra of xMnO·(100-x)[4TeO2·PbO2] glasses in function of manganese oxide content

By introduction of low MnO content (1%) in the host matrix implies the modifications in UV-VIS spectrum: the absorption band situated at ~300 nm is shifting to higher wavelength (315nm) and a larger band appears at about 326 nm which can be due to $^5E_g \rightarrow ^5T_{2g}$ transition of Mn^{+3} ions [85]. Then, the intensity of the band situated at about 260 nm increases. This band is due to $^6A_{1g}(S) \rightarrow ^4A_{2g}(F)$ absorption transitions of Mn^{+2} ion which exists in the UV region in absorption spectrum [86]. The high UV–VIS absorbances between 300 and 400 nm are consistent with the presence of high-valent Mn species.

The high-intensity band centered at 380 and 500 nm can be assigned to oxygen-manganese charge transfer transition from the oxygen ligand to Mn (III). The bands in the region ranging from 350 to 700 nm are not the simple d-d transitions for octahedrally coordinated Mn (III) ions. A similar band is centered at about 950nm which is almost independent of the nature of the remaining oxygens ligands.

4.5.4. EPR spectroscopy

The spectra consist mainly of resonance lines centered at g–factor values of geff ≈2.0 and geff ≈4.3, their relative intensity depending on the manganese content of the samples as shown in figure 4.21.

The strongly distorted versions of the octahedral vicinity, subjected to strong crystal field effects, give rise to absorptions at geff≈4.3. The absorption line centered at geff≈2.0 may be attributed to Mn^{2+} species interacting by magnetic coupling, dipolar and/ or super exchange, the last ones forming magnetic clusters.
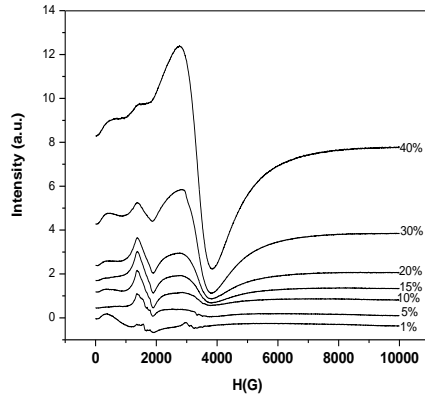
Fig. 4.21. EPR spectra due to Mn2+ ions in xMnO·(100-x)[4TeO$_2$·PbO$_2$] glasses for $1 \leq x \leq 40$ % mol

For x≤5 mol % the EPR spectrum consists in absorption lines centered la g≈4.3 and g ≈2.0 values. The hfs were resolved on both g≈4.3 and g≈2.0 obsorptions due to the nuclear spin (I=5/2) interaction (Figure 4.21.)

The intensity and the line - width of the resonance line at geff≈4,3 for all investigated systems is represented in figure 4.22 (a,b).

Fig. 4.22. The dependence on MnO content of the intensity (a) and width (b) of resonance line at gef ≈4.3 for xMnO·(100-x)[4TeO$_2$·PbO$_2$] glasses for $1 \leq x \leq 40$ % mol

The intensity of the resonance line at geff≈4.3 can be observed as increasing up to 15 mol % (Figure 4.22.a), over this concentration, the intensity decreases. The line - width of the resonance line at geff≈4.3 (Figure 4.22.b) decreases with the increase of x in the whole concentration range.

The non-linear increase of intensity (Figure 4.23.) with MnO concentration shows that manganese ions are present as Mn^{2+} as well as Mn$^{3+.}$ The line - width of the resonance line from geff≈2.0 (Figure 4.23.b).) increases up to 5 % mol due to manganese species interacting by magnetic coupling dipole-dipole as the main broadening mechanism. Over this concentration line -the width of the resonance line from gef≈2.0 decreases due to interacting superexchange between the manganese ions.
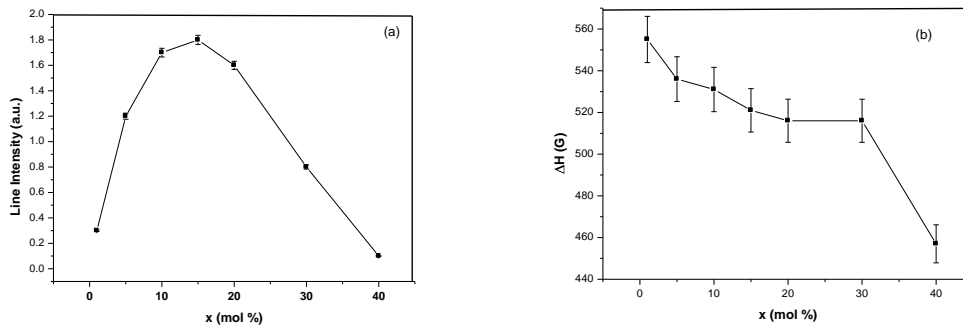
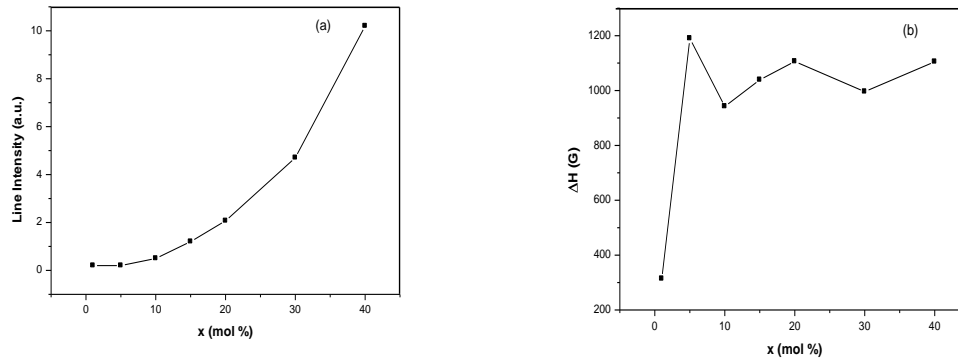Fig. 4.23. The dependence on MnO content of the intensity (a) and width (b) of resonance line at gef ≈2.0 for xMnO·(100-x)[4TeO$_2$·PbO$_2$] glasses for $1 \leq x \leq 40$ % mol

CHAPTER 5. Characterization of some tellurite glasses doped with rare earth ions and transitional ions obtained by sol-gel method

5.1. The preparation and processing of the samples

The glass systems: TeO$_2$·xEu$_2$O$_3$, x=1,6-32 % mol, TeO$_2$·xGd$_2$O$_3$, x=8-32 % mol, TeO$_2$·xFe$_2$O$_3$, x=8-40 % mol, TeO$_2$·xCuO, x=3,2-48 % mol, TeO$_2$·xMnO, x=3.2-64 % mol were prepared using sol-gel method, using Te(OEt)$_4$, Eu(NO$_3$)$_3$×6H$_2$O, Gd(NO$_3$)$_3$×6H$_2$O, Fe(NO$_3$)$_3$×9H$_2$O, Cu(NO$_3$)$_2$×3H$_2$O, Mn(NO$_3$)$_2$×4H$_2$O as precursors, CH$_3$COOH and EtOH as solvents. Tellurium (IV) ethoxide was dissolved in ethanol, followed by addition of iron (III) nitrate and glacial acetic acid under continuous stirring until the reaction mixture became homogeneous. Then, the reaction mixture was stirred for 45 minutes at 60 ºC in atmospheric conditions. After filtration, the wet gel obtained was dried in the oven for 24 hours at 80 ºC, and was ground to give fine powder.

5.2. Characterization of tellurite system doped with iron ions

5.2.1. X-ray diffraction

XRD analysis of the structure of tellurite systems obtained showed no distinguishing peaks, which indicates that systems were amorphous (Fig. 5.1.)
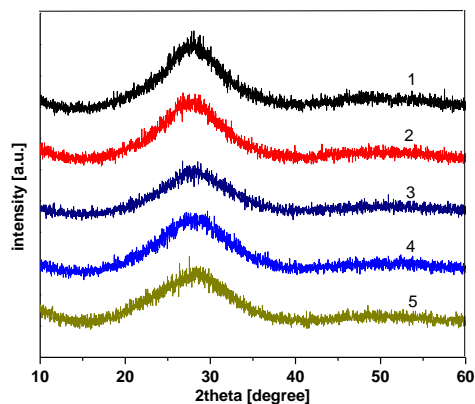
Fig.5.1. X-ray diffraction patterns for iron-tellurite glass samples.

5.2.2. FTIR spectroscopy

A simple inspection of the spectral features presented in Figure 5.2 shows that because the majority of the bands are large and asymmetric, presenting also some shoulders, a deconvolution of the experimental spectra was necessary. The deconvoluted IR spectra for the iron-tellurite glasses are shown in Figure 5.2. and the peak assignments are given in Table 5.2. This deconvoluted allowed us a better identification of all bands that appear in the FTIR spectra in order to realize their assignment. The deconvoluted procedure was made by using the Spectra Manager program [19] and a Gaussian type function.
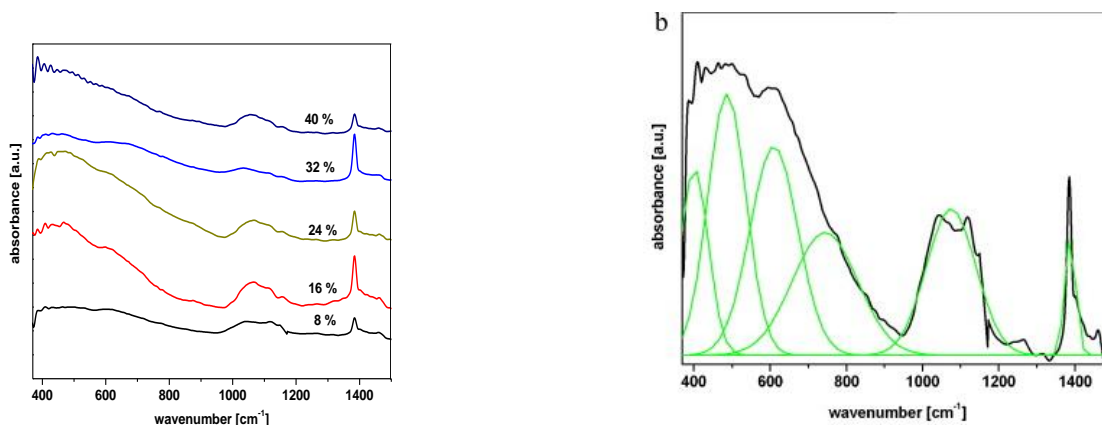
Fig. 5.2. a) FTIR spectra of iron-tellurite glass samples obtained by sol-gel method; b) Deconvoluted FTIR spectrum for x = 8 % mol Fe_2O_3

Table 5.2. Deconvolution parameters (the band centers C and the relative area A) and the bands assignments for the iron-tellurite glasses.

Sample 1		Sample 2		Sample 3		Sample 4		Sample 5		Assignments
A	C	A	C	A	C	A	C	A	C	
2.68	418	11.50	421	7.12	418	3.09	405	7.79	386	Bending vibrations of Te-O-Te sau

										O-Te-O linkages [7]
3.96	521	7.35	531	15.61	529	8.33	503	6.72	495	Fe-O vibrations of [FeO$_4$] and [FeO6][8]
3.32	618	3.99	631	4.68	692	3.19	662	6.17	628	Stretching vibrations of [TeO$_4$] structural units [9]
2.82	757	2.44	722	5.09	758	5.05	774	4.57	772	Stretching vibrations of [TeO$_4$] structural units [10]
3.31	1078	2.4	1076	2.19	1079	1.31	1049	1.87	1070	C- O stretching in alcohol [11]
1.6	1390	1.39	1386	0.57	1386	0.75	1384	0.46	1390	Stretching vibrations of NO$_3^-$ group/methyl group [12]

By increasing of Fe_2O_3 content ($x \geq 24$ mol % Fe_2O_3) increases the number of [TeO$_4$] and [TeO$_3$] structural units. The increasing trends in the intensity of these bands can be due to the formation of bridging bond of Te-O-Te and O-Te-O linkages.

5.2.3. UV-Vis spectroscopy

The bands located in the 300-450 nm region are due to the presence of the Fe[+3] ions. These bands can be due to the d-d transitions of the Fe[+3] ions.
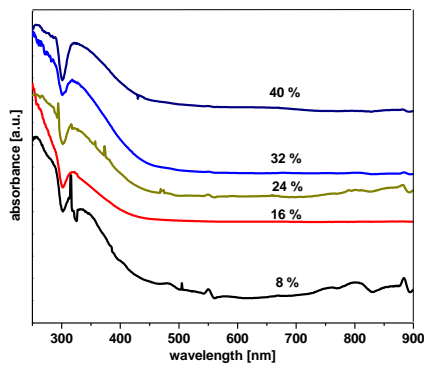
Fig. 5.4. UV-VIS absorption spectra of iron-tellurite systems

For x = 8 mol % Fe_2O_3 si x = 24 mol % Fe_2O_3 some modifications of the bands appear in this region. Then, the apparition of new bands located in the 260-325nm region is correlated to the possible distortions of symmetry of the iron species. The bands located in the 250-277nm region are due to a strong oxygen-iron charge transfer derived to the Fe+2 and Fe+3 ions.

For x = 8 mol % , three absorption bands located at about 540, 583 and 785nm are identified due to transitions: $^6A_1(e^2t_2^3) \rightarrow a^4T_1(e^3t_2^2)$(spin forbidden), $A_1(t_{2g}^3e_g^2) \rightarrow a^4T_2(t_{2g}^4e_g)$, $^6A_1(t_{2g}^3e_g^2) \rightarrow a^4T_1(t_{2g}^4e_g)$.

A very sharp absorption band is observed at about 320nm only for x=8 mol % Fe_2O_3.

Fe^{+2} ions produce a band due to oxygen-iron charge transfer in the ultraviolet [16].

Spin-forbidden bands are also expected in the 450-550 nm domain. Then, Fe^{+2} ions yield absorption bands due to d-d transitions in the near infrared region and can be attributed to a range of distorted octahedral sites. Accordingly, the energy diagram of the $3d^6$ configuration (Fe^{+2}) indicates that its spectrum will consist essentially of a single band in the infrared region as well as a number of very weak spin-forbidden bands in the visible and ultraviolet regions. For x = 8 mol % Fe_2O_3 and x = 24 mol % Fe_2O_3, the intensity of the bands situated in the infrared region show that some Fe^{+3} ions were converted to Fe^{+2} ions.

5.2.4. EPR spectroscopy

The Fe^{3+} EPR spectra (Figure 5.5.) are characterized by resonance absorptions at g ≈ 4,3 and g ≈ 2,0, their relative intensity depending on the iron content of the samples. The resonance line at g ≈ 4,3 is corresponding to the isolated Fe^{3+} ions situated in octahedral, rhombic or tetragonal symmetric distorted neighborhoods. The line from gef ≈ 2,0 is attributed to Fe^{3+} ions involved in magnetic interactions or clusters.
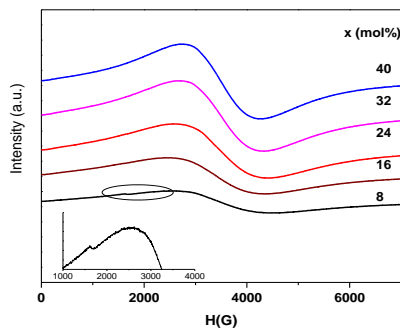

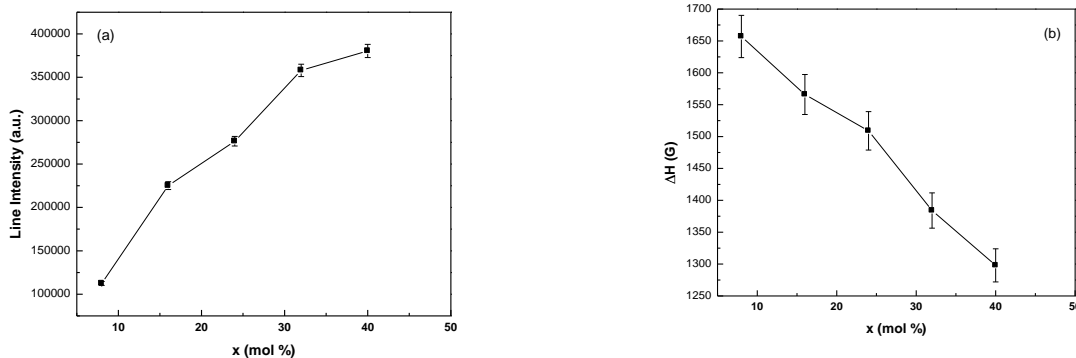Fig. 5.5. EPR spectra due to Fe^{3+} ions in iron-tellurite systems

Fig. 5.6. The dependence on Fe_2O_3 content of the intensity (a) and width (b) of resonance line at gef ≈2.0 for iron-tellurite systems

The intensity of the resonance line at geff ≈ 2.0 (Figure 5.6.a) increases with the increase of x in the whole concentration range. The non-linear increase of intensity with iron concentration shows that iron ions are present as Fe^{2+} as well as Fe^{3+}. The line - width of the resonance line from geff≈2.0 (Figure 5.6.b).) of x in the whole concentration range due to could appear superexchange interactions.

In figure 5.7. are presented the temperature dependence of integral intensity for iron-tellurite systems. It could be observed that these dependence are linear typical for Curie-Weiss low. From these dependence one could evaluate the paramagnetic Curie temperature θ_p. The evaluated temperatures are presented in Figure 5.8. All evaluated θ_p are negative values, characteristic to antiferromagnetic coupled ions by means of super exchange interactions.

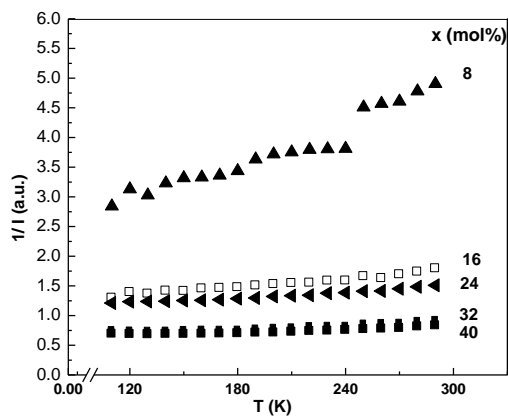

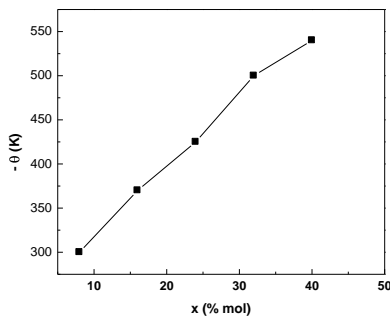Fig. 5.7. Temperature dependences of 1/I for iron-tellurite systems

Fig. 5.8. Concentration dependence of θ_p for iron-tellurite systems

5.3. Characterization of tellurite system doped with europium ions

5.3.1. X-ray diffraction

XRD analysis of the structure of tellurite systems obtained showed no distinguishing peaks, which indicates that systems were amorphous (Fig. 5.9.)
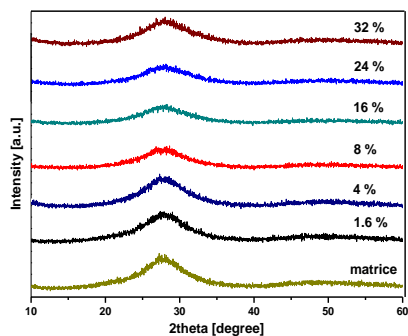
Fig. 5.9. X-ray diffraction patterns for europium-tellurite systems.
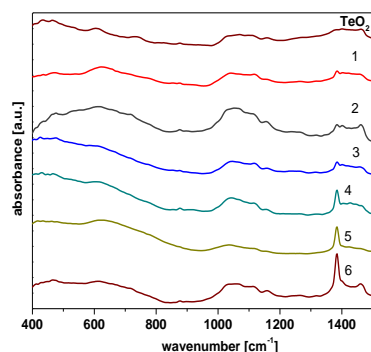
5.3.2. FTIR spectroscopy

Fig.5.10. FTIR spectra of europium-tellurite systems

Table 5.3. Wavenumbers and their assignments for FTIR spectra of europium-tellurite systems

$\nu(cm^{-1})$	Assignments
432	Vibrations of Te-O in [TeO$_6$] structural units
470	Bending vibrations of Te-O-Te linkages
607	Vibrations of Te-O in [TeO$_6$] structural units
625-680	Stretching vibrations of [TeO$_4$] structural units
740-780	Stretching vibrations of [TeO$_3$] structural units
1000-1200	C- O stretching in alcohol
1380	Stretching vibrations of NO^{3-} group/methyl group

The IR results suggest that six-coordinated tellurium (VI) in [TeO$_6$] structural units were partially changed to four-coordinated tellurium (IV) in [TeO$_4$] structural units during doping with Eu$_2$O$_3$.

For x=6-16 mol % Eu$_2$O$_3$, a sharp decreasing trend was observed both in wavenumber and strength of the band situated between 400 and 800cm^{-1}, which might be due to the formation of the Eu-O-Te bridging bonds. Since the stretching force constant of Eu-O bonding is substantially lower than that of the Te-O, the stretching frequency of Eu-O-Te might trend to be lower.

The adding of 24 mol % Eu$_2$O$_3$ gives rise of the non-bridging oxygens because some [TeO$_4$] structural units were transformed in [TeO$_3$] structural units. Then, bands situated at about 625 and 780

cm^{-1} move towards larger wavenumber and they appear broader. This shift could be attributed to the Eu^{+3} ions incorporation as network modifiers which form new non-bridging oxygens in Te-O$^-$ …Eu^{+3}….O$^-$-Te linkages. This shows that the europium ions are firstly inserted in the trivalent state and they can be considered as modifiers because they have a strong affinity towards these groups containing non-bridging oxygens, with negative electric charges.

By increasing of the Eu$_2$O$_3$ concentration up to 32 mol%, the conversion of some [TeO$_4$] into [TeO$_3$] structural units was observed again because the europium ions have a strong affinity towards these groups containing non-bridging oxygens, with negative electric charges. The modifications of the absorption bands corresponding to the Te-O-Te bending modes situated at about 470 cm^{-1} are proofs of these affinities.

5.3.3. UV-Vis spectroscopy

Absorption of Eu^{+3} in TeO$_2$ sol-gel systems is given in Figure 5.11. The stronger transitions in the UV-VIS spectrum can be due to the presence of the Te=O bonds from [TeO$_3$] structural units which allow n-π^* transitions.
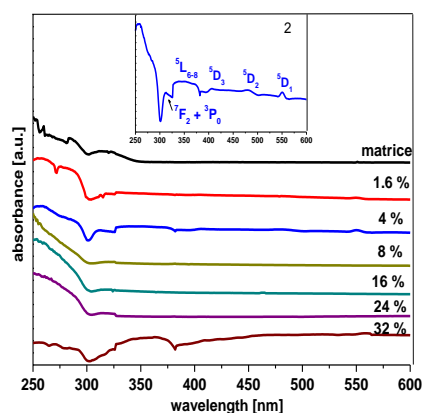
Fig. 5.11. UV-Vis spectra of europium-tellurite systems

Table 5.4. Assignments of Eu^{3+} absorption bands in the europium-tellurite systems

x [mol %]	Wavelength [nm]	Assignments
1.6-32	308	$^7F_0 \rightarrow ^7F_2$
1.6-32	312	$^7F_0 \rightarrow ^5H_6$
1.6-32	320	$^7F_0 \rightarrow ^5H_4$
1.6-32	328	$^7F_1 \rightarrow ^5H_7$
8, 24	362	$^7F_0 \rightarrow ^5D_4$
1.6	376	$^7F_0 \rightarrow ^5G_4$

1.6, 4, 16	383	$^7F_0 \rightarrow {}^5G_2$
1.6, 4, 8	404	$^7F_1 \rightarrow {}^5L_6$
24	410	$^7F_0 \rightarrow {}^5D_3$
8, 24	463	$^7F_0 \rightarrow {}^5D_2$
1.6, 4, 24	550	$^7F_0 \rightarrow {}^5D_1$

5.4. Characterization of tellurite system doped with gadolinium ions

5.4.1. X-ray diffraction
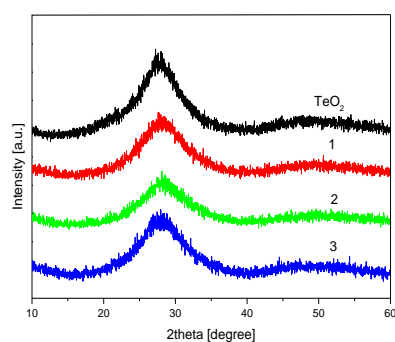
Fig. 5.12. X-ray diffraction patterns for gadolinium-tellurite systems.
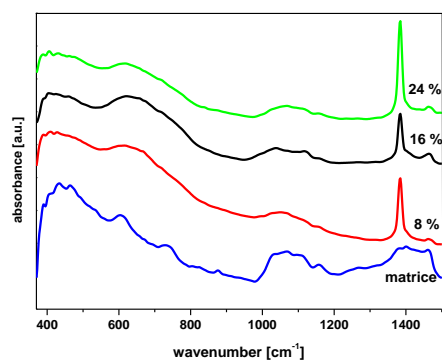
Fig. 5.13. FTIR spectra of gadolinium-tellurite systems

XRD analysis of the structure of tellurite systems obtained showed no distinguishing peaks, which indicates that systems were amorphous (Figure 5.12.)

5.4.2. FTIR spectroscopy

The FTIR spectra of gadolinium-tellurite systems are shown in Figure 5.13.

Table 5.5. Wavenumbers and their assignments for FTIR spectra of gadolinium-tellurite systems

ν (cm^{-1})	Assignments
434	vibrations of Te-O in [TeO$_6$] structural units
460-464	bending vibration of Te-O-Te linkages
540	Vibrations of Te-O$^-$

605	vibrations of Te-O in $[TeO_6]$ structural units
616-675	stretching vibrations if $[TeO_4]$ structural units
730	stretching vibrations of $[TeO_3]$ structural units
1000-1300	C-O stretching in alcohols
1380	methyl symmetrical C–H bending or asymmetric stretching vibrations of NO_3^- group
1462	methyl asymmetrical C–H bending

The absorption band situated at 605 cm^{-1} in the host matrix is shifting to higher wavenumbers (616 cm^{-1}) by dopping of Gd_2O_3. A shift of absorption band to higher wavenumber indicates the conversion of some $[TeO_6]$ to $[TeO_4]$ structural units.

The bands centered at 1380 cm-1 and 1462 cm^{-1} can be due to the methyl group. The absorption band situated at about 1380 cm^{-1} belongs to the asymmetric stretching vibrations of NO_3^- group, revealing that nitrate in the as-prepared samples does not decompose at 80 °C yet.

5.4.3. UV-Vis spectroscopy

UV-Vis spectra of the studied samples are presented in Fig. 5.14. The analysis of UV-VIS spectra can see that the position of absorption bands is shifted to higher wavelengths with increasing concentration of gadolinium ions. Stevels [50] suggest that the absorption bands shift to higher wavelengths correspond to transitions from non-bridging oxygens oxygen linking an excited electron less tightly than an atom of bridging oxygen.
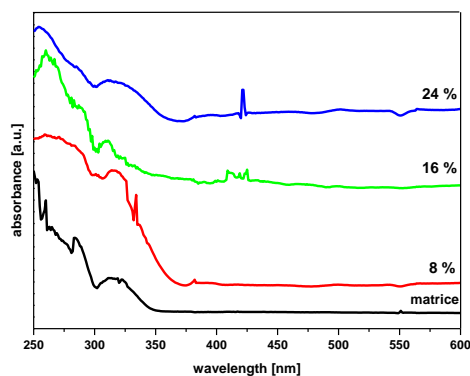
Fig. 5.14. UV-Vis spectra of gadolinium-tellurite systems

The stronger transitions in the UV-VIS spectrum can be due to the presence of the Te=O bonds from $[TeO_3]$ structural units which allow n-π^* transitions.

Absorption bands in 250-260 nm region are due to transitions of charge transfer (CT) oxygen-Gd^{3+} [51, 52]. CT transitions occur when a valence electron is transferred from the ligand to the unoccupied orbital of the metal cation. The absorption spectra of tellurite system consist of bands attributable to f-f transitions between the ground state of Gd^{3+} (^8S) and multipletii ^6P_J, ^6I_J and $_6D_J$.

5.4.4. EPR spectroscopy

The spectrum consist one of resonance lines centered at g≈2.0, due to clustered ions.

Fig. 5.15. EPR spectra due to gadolinium ions in gadolinium-tellurite systems

5.5. Characterization of tellurite system doped with copper ions

5.5.1. X-ray diffraction

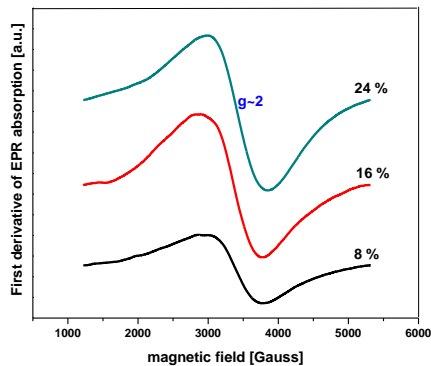No peaks are observed in XRD pattern confirming the amorphous nature of the studied samples (Figure 5.16.).
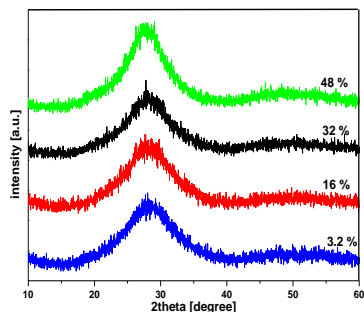
Fig. 5.16. X-ray diffraction patterns for copper-tellurite systems.

5.5.2. FTIR spectroscopy

The FTIR spectra of the samples (Figure 5.17.) are characterized by intense absorption bands in the frequency regions 400-500 cm^{-1}, 604-680 cm^{-1}, 720-780 cm^{-1}, 1000-1500 cm^{-1}. The examination of the FTIR spectra shows that the CuO content modifies the characteristic IR bands.

The bands located in the spectral range 404-500 cm^{-1}, 620-680 cm^{-1} and 720-775 cm^{-1} are assigned to the bending mode of Te-O-Te or O-Te-O linkages, to the stretching mode [TeO$_4$] trigonal pyramidal with bridging oxygen and to the stretching mode of [TeO$_3$] trigonal pyramidal with non-bridging oxygen, respectively.

Fig. 5.17. FTIR spectra of copper-tellurite systems

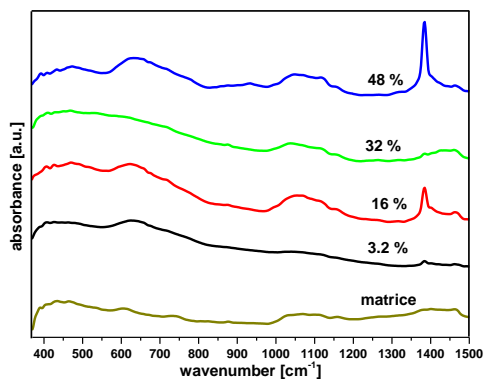The absorption band situated at 604 cm^{-1} is shifted to higher wavenumbers (630 cm^{-1}) by introduction of CuO content (x=3.2 mol %). Usually, a shift of absorption bands to higher frequencies occurs as a result of an increase in the degree of polymerization of the structural network of the glass. Therefore, the FTIR results suggest that six-coordinated tellurium (VI) in [TeO_6] structural units were partially changed to four-coordinated tellurium (IV) in [TeO_4] structural units during doping with CuO.

By increasing of CuO content up to 16 mol % (sample 2) increases the number of [TeO_4] and [TeO_3] structural units. The increasing trends in the intensity of these bands can be due to the formation of bridging bond of Te-O-Te and O-Te-O linkages.

The FTIR absorption spectra observed for copper nitrate - tellurate glasses revealed the presence of two bands at around 656 cm^{-1} and 675 cm^{-1}, accompanied by a shift to higher wave number, indicating the appearance of TeO_3 units corresponding to a reduction in the number TeO_4 units.

For x=32 mol % we can be observed that the addition of copper ions is leading to a broadening of the bands located in the 400-800 cm^{-1} region and to a structure more and more disordered. This might can be due to the formation of the Cu-O-Te bridging bonds.
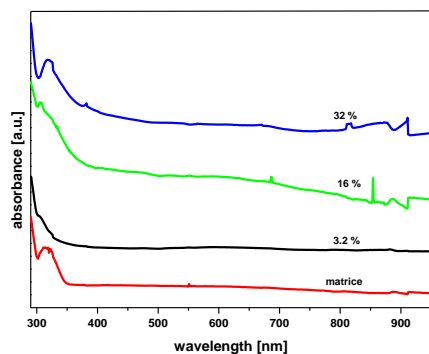
5.5.3. UV-Vis spectroscopy

Fig. 5.18. UV-Vis spectra of copper-tellurite systems

The observed band at ~ 815 nm (x=32 mol %) is due to transitions $^2B_{1g} \rightarrow {}^2B_{2g}$. This band can be identified as the d-d transitions due to Cu^{2+} ions and described in terms of the ligand field theory [71]. The located band at 680 nm (x=16-32 mol %) is attributed to Cu^{2+} ion present in the sample. This absorption may be due to $^2T_{2g} \rightarrow {}^2E_g$ transition of Cu^{2+} [72]. It can also be observed at 390 nm absorption band (x=16-32 mol %) due to transitions ($^2B_{1g} \rightarrow {}^2E_g$) of copper ions Cu^{2+} [73.74]. Bands located at ~ 615 nm (all samples), ~ 867 nm (x=16-32 mol %) are attributed to $^2B_{2g} \rightarrow {}^2A_{1g}$ transitions of Cu^{2+} ions [75].

5.5.4. EPR spectroscopy

The spectra show the parallel partially resolved hfs due to the interaction of the unpaired electron with the nuclear spin I=3/2 of the Cu^{2+} ion. The perpendicular hfs is not resolved indicating a width of the individual components exceeding the $|A_\perp|$ separation. For higher concentrations, EPR spectra show a single absorption line due to clustered ions Cu^{2+}, located at $g \approx 2.1$.
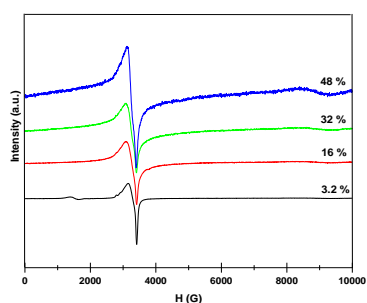

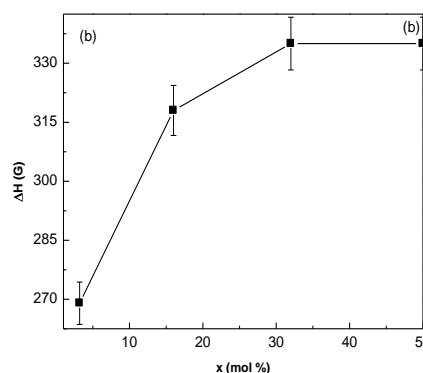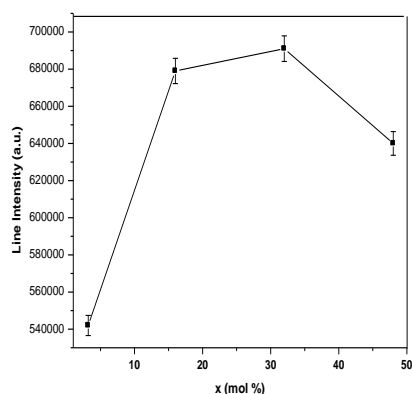Fig. 5.19. EPR spectra due to copper ions in copper-tellurite systems

Fig. 5.20. The dependence on CuO content of the intensity (a) and width (b) of resonance line at geff ≈ 2.1 for copper-tellurite systems

The intensity of the resonance line at geff ≈ 2.1 can be observed as increasing up to 32 mol % (Figure 5.20.a). Over this concentration, the intensity decreases due to decrease in the number of Cu^{2+} ions.

The gef ≈2.1 resonance line-width (Figure 5.20.b) increases up to 32 mol % CuO, where a change of slope takes place, due to the dipolar interactions. For higher concentrations (x≥32 mol %) the increase of line-width is attenuated and this supports the existence of exchange interaction between Cu^{2+} ions.

In figure 5.21. are presented the temperature dependence of integral intensity for copper-tellurite systems.
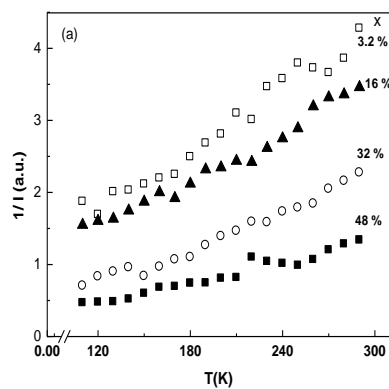
Fig. 5.21. Temperature dependences of 1/I for copper-tellurite systems.

All evaluated θp are negative values. In the low range of CuO concentrations these values are closed to 0 K, from where results that in this composition range copper ions presents are isolated and presents a paramagnetic behavior. For higher concentration of CuO, antiferromagnetic behavior is increasing.

5.6. Characterization of tellurite system doped with manganese ions

5.6.1. X-ray diffraction

No peaks are observed in XRD pattern confirming the amorphous nature of the studied samples (Figure 5.16.).
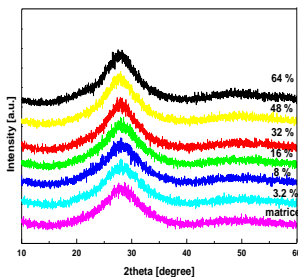
Fig. 5.22. X-ray diffraction patterns for manganese-tellurite systems.

5.6.2. FTIR spectroscopy
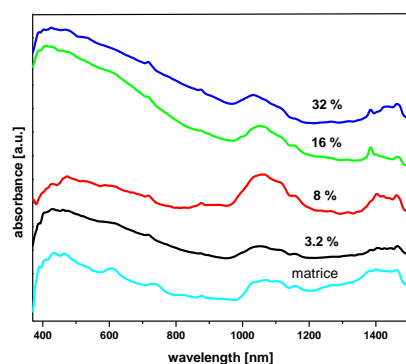
Fig. 5.23. FTIR spectra of manganese-tellurite systems

The IR results suggest that six-coordinated tellurium (VI) in $[TeO_6]$ structural units were partially changed to four-coordinated tellurium (IV) in $[TeO_4]$ structural units during doping with MnO.

Table 5.6. Wavenumbers and their assignments for FTIR spectra of manganese-tellurite systems

| ν (cm^{-1})	Assignments
420	Vibrations of Mn-O in [MnOn]
435	vibrations of Te-O in $[TeO_6]$ structural units
475	bending vibrations of Te-O-Te linkages
605	vibrations of Te-O in $[TeO_6]$ structural units
730-780	stretching vibrations of $[TeO_3]$ structural units
620-680	stretching vibrations of $[TeO_4]$ structural units
1000-1300	C-O stretching in alcohols
1380	methyl symmetrical C–H bending or asymmetric stretching vibrations of NO3- group
1462	methyl asymmetrical C–H bending

5.6.3. UV-Vis spectroscopy

The stronger transitions in the UV-VIS spectrum can be due to the presence of the Te=O bonds from $[TeO_3]$ structural units which allow n-π^* transitions.
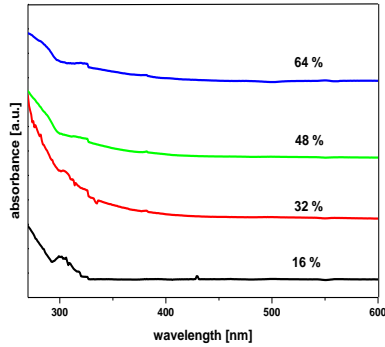
Fig. 5.24. UV-Vis spectra of manganese-tellurite systems

The absorption bands due to of ion Mn^{2+} are located at 293 nm, 325 nm, 378 nm, 392 nm, 428 nm, 460 nm, 530 nm si sunt atribuite tranzitiilor $^6A_{1g}(S)\rightarrow^4T_{1g}(P)$ [101], $^6A_{1g}(S)\rightarrow^4E_g(D)$ [101], $^6A_{1g}(S)\rightarrow^4E_g(D)$ [102], $^6A_{1g}(S)\rightarrow^4T_{2g}(D)$ [102], $^6A_{1g}(S)\rightarrow^4A_{1g}(G)$, $^4E_g(G)$ [102], $^6A_{1g}(S) \rightarrow ^4T_{1g}(G)$ [103], $^6A_{1g}(S) \rightarrow ^4T_{1g}(G)$ [104].

5.6.4. EPR spectroscopy
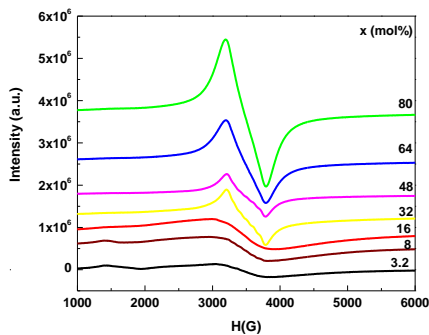
Fig. 5.25. EPR spectra due to manganese ions in manganese-tellurite systems

The spectra consist mainly of resonance lines centered at g–factor values of geff≈2.0, geff≈4.3, their relative intensity depending on the manganese content of the samples as shown in Figure 5.25. This isotropic signal at geff≈2.0 is due to isolated Mn^{2+} ions in an environment close to octahedral symmetry.

The non-linear increase of intensity (Figure 5.26. a) with MnO concentration shows that manganese ions are present as Mn^{2+} as well as Mn^{3+}.
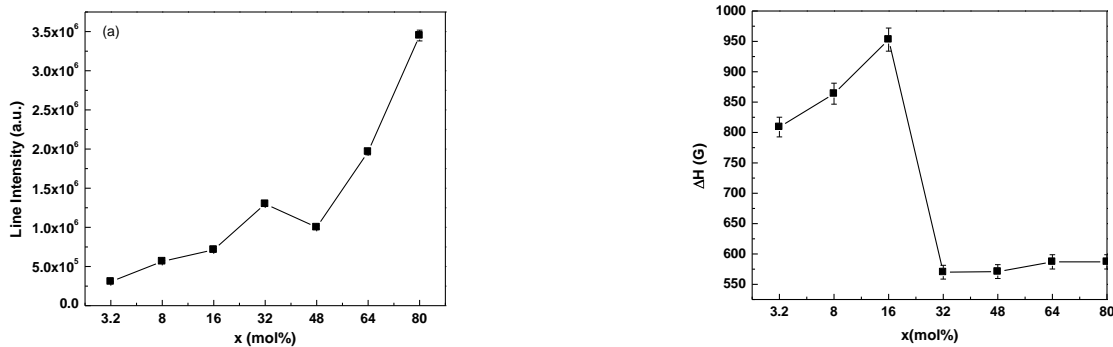
Fig. 5.26. The dependence on MnO content of the intensity (a) and width (b) of resonance line at geff ≈ 2.0 for manganese-tellurite systems

In case of geff ≈ 2.0 absorptions (Figure 5.26.b) for x≤16 mol % the line broadene as result of dipolar interactions between manganese ions. For x>0.16 mol % this broadening is stopped by the exchange narrowing. For x>32 mol % the broadening of the geff ≈ 2.0 absorption line can be explained by the increased role of the Mn^{3+} ions and of the disorder determined by the increase of the MnO content.

All evaluated θ_p are negative values. In the low range of MnO concentrations these values are closed to 0 K, from where results that in this composition range manganese ions presents are isolated and presents a paramagnetic behavior. For higher concentration of MnO, antiferromagnetic behavior is increasing.

Fig. 5.27. Temperature dependences of 1/I for manganese-tellurite systems

SELECTED REFERENCES

CHAPTER 4

- S. Mandal, S. Hazra, A. Ghosh, J. Mater. Sci. Lett. 13 (1994) 1054

- S. Hazra, A. Ghosh, J. Mater. Res. 10(9) (1995) 2374

- S. Rada, **A. Dehelean**, E. Culea, FTIR, Raman and UV-VIS spectroscopic and DFT investigation of the structure of iron-lead-tellurate glasses, Journal of Molecular Modelling, doi: 10.1007/s00894-010-0911-5

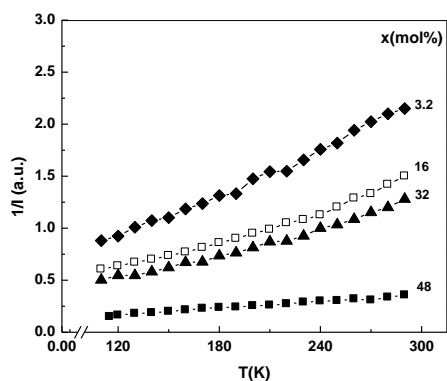- S. Rada, **A. Dehelean**, E. Culea, FTIR and UV-VIS spectroscopy investigation on the europium-lead-tellurate glasses, Journal of Non-Crystalline Solids, doi: 10.1016/j.jnoncrysol.2011.04.013

- S. Rada, M. Culea, E. Culea, J. Phys. Chem. A 112(44) (2008) 11251

- G. Upender, V. G. Sathe, V. C. Mouli, Phys B 405 (2010) 1269–1273

- H . Jia, G. Chen, W. Wang, Opt Mater 29 (2006) 445–448

- T. Sekiya, N. Mochida, S. Ogawa, J. Non- Cryst. Solids 176 (1994) 105

- S. Rada, E. Culea, V. Rus, M. Pica, M. Culea, J. Mater. Sci. 43 (2008) 3713

- E. Burzo, I. Ardelean, I. Ursu, Mater. Lett. 26 (1996) 103

- S. Rada, **A. Dehelean**, E. Culea, Dual role of the six-coordinated lead and copper ions in structure of the copper–lead-tellurate glasses, Journal of Alloys and Compounds, Volume 509, Issue 2, (2011), 321-325

- E. R. Barney, A. C. Hannon, D. Holland, D. Winslow, B. Rijal, M. Affatigato, S. A. Feller, J Non-Cryst Solids 353 (2007) 1741–1747

- T. Castner, G. S. Newell, W. C. Holton, C. P. Slichter, J.Chem. Phys. 32 (1960) 668

- Ardelean, C. Andronache, C. Campean, P. Pascuta, Mod. Phys. Lett. B 45 (2004) 1811

- C. Prakash, S. Husain, R. J. Singh, S. Mollah, J. Alloys Compon. 326 (2001) 47

- S. Rada, **A. Dehelean**, M. Culea, E. Culea, Dinuclear manganese centers in the manganese-lead-tellurate glasses, Spectrochimica Acta Part A: Molecular and Biomolecular Spectroscopy, doi:10.1016/j.saa.2011.02.025

- S. Rada, R. Chelcea, M. Culea, **A. Dehelean**, E. Culea, Experimental and theoretical investigations of the copper–lead–germanate glasses, Journal of Molecular Structure, Volume 977, Issues 1-3, (2010), 170-174

CHAPTER 5

- Introduction to Sol-Gel Processing, by Alain C. Pierre, Kluwer Academic Publishers, Boston / Dordrecht/ London, 2002
- J. C. F. Ng., Y. S. Park, H. F. Shurvell, Spectrochim. Acta, 48A (1992) 1139
- Microcal (TM) Origin, Version 6.0, Microcal Software, Inc., Northampton, MA 01060, USA
- M. Efimov, J. Non-Cryst. Solids, 253 (1999) 95
- S. Rada, **A. Dehelean**, M. Stan, R. Chelcea, E. Culea, Structural studies on iron–tellurite glasses prepared by sol–gel method, Journal of Alloys and Compounds, Volume 509, Issue 1, (2011), 147-151
- H. Wei, J. Lin, W. Huang, Z. Feng, D. Li, Mater. Sci. Eng. B 164 (1) (2009) 51
- L. Weng, S. Hodgson, X. Bao, K. Sagoe-Crentsil, Mater. Sci. Eng.B 107 (2004) 89
- Stuart, Infrared Spectroscopy: Fundamentals and applications, John Wiley&Sons, The Attrium, Southern Gate, Chichester, West Sussex PO 198SQ, England, ISBN 0-470-85427-8 (2004)
- N. Wadaa, K. Kojimab, J. Luminesc. 126 (2007) 53
- S. Hazarika, S. Rai, Opt. Mater. 27 (2004) 173
- K. Annapurnaa, M. Dasa, P. Kundua, R.N. Dwivedia, S. Buddhudub, J. Molec. Struct. 741 (2005) 53
- R.T. Karunakaran, K. Marimuthu, S. Surendra Babu, S. Arumugam, Solid State Sciences 11 (2009) 1882
- S. Jayaseelan, N. Satynarayana, M. Venkateswarlu, Materials Science and Engineering B, vol 106, issue 1 (2004)
- P. Gayathri Pavani, K. Sadhana, V. Chandra Mouli, Physica B 406 (2011) 1242
- L. Armelao, S. Quici, F. Barigelletti, G. Accorsi, G. Bottaro, M. Cavazzini, E. Tondello, Materials. Coordin. Chem. Rev. 254 (2010) 487
- J.G. Bunzli, S. Comby, A. Chauvin, C.D.B. Vandevyver, J. Rare Earths 25 (2007) 257
- S. Mukherjee, P. Dasgupta, P.K. Jana, J. Phys. D Appl. Phys. 41 (2008) 1
- E. Culea, A. Pop and I. Cosma, J. Magn. Magn. Mater. 157/158 (1996) 163
- D.K. Durga, N. Veeraiah, Bull. Mater. Sci 24 (4), 421 (2001)

SELECTED CONCLUSIONS

The main idea of the thesis was to obtain tellurite systems doped with rare earth ions and transitional metal ions by melt/quenching and sol-gel methods.

$xEu_2O_3 \cdot (100-x)[4TeO_2 \cdot PbO_2]$ where x=0-50 mol % Eu_2O_3, $xFe_2O_3 \cdot (100-x)[4TeO_2 \cdot PbO_2]$ where x=0-60 mol % Fe_2O_3, $xCuO \cdot (100-x)[4TeO_2 \cdot PbO_2]$ where x=0-40 mol % CuO, glasses were prepared by melting/quenching.

A series of tellurite systems were prepared by sol-method. Tellurium (IV) ethoxide (85 %) and stoichiometric quantities of $Eu(NO_3)_3 \times 6H_2O$, $Gd(NO_3)_3 \times 6H_2O)$, $Fe(NO_3)_3 \times 9H_2O$, $Cu(NO_3)_2 \times 3H_2O$, $Mn(NO_3)_2 \times 4H_2O$, absolute ethanol and glacial acetic acid, were employed for sol-gel method.

In the present study, tellurite systems were studied by density measurements, FTIR, UV-Vis and EPR spectroscopy.

The summary of the conclusions drawn from the investigation on tellurite glasses obtained by *melt/quenching* is as follows:

- ✓ XRD analysis of the structure of tellurite glasses obtained showed no distinguishing peaks, which indicates that systems were amorphous.
- ✓ The values of density suggested important structural modifications of the vitreous network.
- ✓ The bands located in the 400-500 cm^{-1} region are attributed to the bending mode of Te-O-Te linkages which may be overlapped with that assigned to the bending mode of the Pb-O-Pb stretch in the $[PbO_4]$ structural units, 620-680 cm^{-1} are assigned to the stretching vibrations of equatorial and axial Te-O bond in the $[TeO_4]$ trigonal bipyramidal units, 670 cm^{-1}, 870 cm^{-1} can be attributed to Pb–O bond vibrations from $[PbO_3]$ and $[PbO_4]$ structural units, 720-780 cm^{-1} are assigned to vibrations of Te-O bond of the $[TeO_3]$ units, absorption bands located at about 1000 and 1100 cm^{-1} are attributed to Pb–O asymmetric stretching vibrations in $[PbO_n]$ structural units. A shift of absorption bands to higher wavenumber indicates the conversion of some $[TeO_4]$ into $[TeO_3]$ structural units, because the lead ions have a strong affinity towards these groups containing non-bridging oxygens, with negative charge. For glasses doped with iron ions, FTIR spectra showed absorption bands due to vibrations of Fe-O bond in the structural units $[FeO_4]$ and $[FeO_6]$.

- The stronger transitions in the UV-VIS spectrum can be due to the presence of the Te=O bonds from [TeO$_3$] structural units and Pb=O bonds from [PbO$_3$] structural units which allow n-π* transitions. The absorption of Pb^{2+}, Eu^{3+}, Eu^{2+}, Fe^{3+}, Fe^{2+}, Cu^{2+}, Cu$^+$, Mn^{2+} si Mn^{3+} ions was emphasized by UV-Vis spectroscopy.

- The distribution of Fe^{3+}, Cu^{2+}, Mn^{2+} ions in several structural units of the glasses was revealed by the EPR spectra, the structure depending of the Fe$_2$O$_3$, CuO and MnO content. The evolution of the spectra is easier to follow considering the dependence of concentration on the EPR parameters, the line - intensity (obtained as an integral of the area under the corresponding EPR signal), J and the line - width, ΔH. The evolution of J and ΔH reflects the structural transformations which appear in the glass matrices due to the increase of iron, copper and manganese ions content.

The summary of the conclusions drawn from the investigation on tellurite glasses obtained by *sol-gel method* is as follows:

- XRD analysis of the structure of tellurite glasses obtained showed no distinguishing peaks, which indicates that systems were amorphous.

- From FTIR absorption spectra of the matrix, it can be observed the bands due to vibrations of Te-O bonds in [TeO$_6$] and [TeO$_3$] structural units. The IR results suggest that six-coordinated tellurium (VI) in [TeO$_6$] structural units were partially changed to four-coordinated tellurium (IV) in [TeO$_4$] structural units during doping with earth rare ions and transitional metal ions.

- The stronger transitions in the UV-VIS spectrum can be due to the presence of the Te=O bonds from [TeO$_3$] structural units. The absorption of Fe^{3+}, Fe^{2+}, Eu^{3+}, Gd^{3+}, Mn^{2+} si Mn^{3+} ions was emphasized by UV-Vis spectroscopy.

- The distribution of Gd3+, Fe^{3+}, Cu^{2+}, Mn^{2+} ions in several structural units of the glasses was revealed by the EPR spectra. The magnetic susceptibility data are in good agreement with the EPR result.

- The EPR spectra of iron-tellurite systems are presented two absorption lines centered at geff≈4.3 and geff≈2.0, the structure depending of the Fe$_2$O$_3$ content. The reciprocal magnetic susceptibility obeys a Curie-Weiss law with negative paramagnetic Curie temperature: (θp) characteristic to antiferromagnetic coupled ions by means of super exchange interactions.

- The EPR spectra of gadolinium-tellurite systems are presented one absorption line centered geff≈2.0 due to clustered ions.

- ✓ The EPR spectra of copper-tellurite systems are asymmetric, characteristic of Cu^{2+} ions in an axially distorted octahedral environment. For $x \leq 16$ % mol CuO, the temperature dependence of the reciprocal magnetic susceptibility obeys a Curie law. In this concentration range the copper ions are predominantly isolated or/and participate in dipole-dipole interractions. At higher concentrations ($x \geq 32$ mol %) the reciprocal magnetic susceptibility obeys a Curie-Weiss law with negative paramagnetic Curie temperature: (θp) characteristic to antiferromagnetic coupled ions by means of super exchange interractions.

- ✓ The EPR spectra of manganese-tellurite systems are presented two absorption lines centered at $g_{eff} \approx 4.3$ and $g_{eff} \approx 2.0$ that can be attributed to Mn_{2+} species. All evaluated θp are negative values. In the low range of MnO concentrations these values are closed to 0 K, from where results that in this composition range manganese ions presents are isolated and presents a paramagnetic behavior. For higher concentration of MnO, antiferromagnetic behavior is increasing.